JOURNAL OF CATALYSIS 25, 378–390 (1972)

The Structure and Activity of Chromium Oxide Catalysts

I. Structure Analysis

STANLEY R. DYNE,* JOHN B. BUTT** AND GARY L. HALLER†

Department of Engineering and Applied Science, Yale University, New Haven, Connecticut 06520

Received September 8, 1971

Two forms of activated chromia catalysts are recognized: (1) an amorphous form, catalyst A, prepared by heating under vacuum or in an inert atmosphere, and (2) a microcrystalline form, catalyst C, prepared by heating in a reducing atmosphere. The structural properties of these catalysts have been studied by X-ray line-broadening, radial distribution analysis, electron microscopy, infrared spectroscopy, and low temperature nitrogen adsorption.

Catalyst C, prepared by heating in hydrogen, is composed of crystallites of α-chromium oxide supported on amorphous chromia. Detailed analysis of the X-ray diffraction powder pattern indicates little contribution to the linewidth from strain. The shape of the crystallites (characterized by X-ray line-broadening of the (104), (110), and (116) diffraction peaks) is oblong. The dimension along the a-axes is roughly twice that along the c-axis. The electron micrographs are consistent with this picture. Attempts to prepare crystallites with dimensions between 15 and 70 Å were unsuccessful. Typically a catalyst activated at 400°C has an effective crystallite size of 80×90 Å while a 450°C activated catalyst has an effective crystallite size of 110×200 Å. The percentage crystalline phase estimated from infrared absorption in the lattice vibration region in catalysts activated for 12 hr at a temperature between 400–450°C are in the range 5–30%.

Catalyst A, prepared by heating in helium, does not give rise to a discernible X-ray diffraction pattern, but does result in a well defined radial distribution curve. Analysis of the radial distribution curve indicates that there exists local order over approximately a 10 Å dimension of the same kind as found in α-Cr_2O_3. A model for this local order is proposed.

INTRODUCTION

Several detailed investigations of specific catalytic activity as a function of dispersion of metal catalysts on support materials have been made in recent years (*1*). With some notable exceptions such as the stereospecific polymerization of α-olefins on α-$TiCl_3$ (*2*) and the extensive work on aluminosilicate catalysts (*3*), however, little attention has been given to the influence of catalyst structure on the activity or selectivity of nonmetallic catalysts. Chromium oxide is representative of the largest class of nonmetallic catalysts, the metal oxides, and it catalyzes a wide variety of hydrocarbon reactions, several of which have been demonstrated to be sensitive to the structure of the catalyst (*4*). Therefore, a simultaneous investigation of the structure of unsupported chromium oxide catalysts and correlation of their reactivity with the deduced structure

* Present address: National Institute for Metallurgy, 1 Yale Road, Milner Park, Johannesburg, South Africa.

** Present address: Department of Chemical Engineering, Northwestern University, Evanston, IL 60201.

† To whom queries concerning this paper should be sent.

might allow us to define more completely the nature of the active centers on these catalysts and perhaps on oxide catalysts generally.

When prepared by the slow heating of the hydrous gel two distinct structures are recognized for chromium oxide (*4*): (i) Catalyst A (amorphous) prepared by heating in a stream of inert gas is characterized by a high surface area (~300 m^2/g) and the absence of a discernible X-ray diffraction pattern; and (ii) catalyst C (crystalline), which is prepared by heating in a stream of hydrogen and is characterized by a low surface area (~100 m^2/g) and an X-ray diffraction pattern consisting of broadened lines indicating the presence of microcrystallites of α-Cr_2O_3. In order to specify the structure of catalyst C more completely, we wish to answer the following questions. What is the average size and shape of the microcrystallites? Can we systematically vary the average size of the crystallites (the critical range of 15–70 Å is of particular interest) (*5*) by varying conditions of preparation such as the hydrogen pressure, heating rate, and final temperature? What fraction of the catalyst is composed of microcrystallites? The structure of catalyst A is in one sense known since there does not exist sufficient long range order to diffract X-rays in the usual manner; and it can thus be said to be amorphous. But it is probably the very short range order (or lack of it) that defines the active centers. Therefore, for catalyst A we ask what the average coordination number is for the oxide and chromium ions. Does there exist some short range order beyond the first coordination sphere and, if so, is it different from that of catalyst C? In the present paper, we give answers obtained to a number of these questions using the following techniques: X-ray line-broadening, electron radial distribution analysis (from X-ray scattering), electron microscopy, infrared spectroscopy, and low temperature nitrogen adsorption (BET). In the following paper (*6*), we report the specific rates of isomerization and hydrogenolysis of cyclopropane and methylcyclopropane and suggest possible correlations with the catalyst structure.

Experimental Methods

Materials. Hydrous chromia gel was prepared by the hydrolysis of urea in a solution of chromium nitrate (reagent grade materials were used) (*7*). The gel was washed repeatedly, filtered, dried in air at 110°C for 16 hr, crushed and sieved to 50/100 mesh. The standard preparation for catalyst C was to heat the air dried gel at a linear rate of 1°C/min to 400°C in flowing hydrogen (20 cc/min). The temperature was maintained at 400°C for 12 hr and the resulting catalyst cooled in flowing hydrogen. The preparation of catalyst A (amorphous) was identical except the hydrogen was replaced by helium above 300°C and the catalyst was cooled to room temperature in helium. Hydrogen was purified by diffusion through a palladium–25% silver thimble supplied by Englehard Industries, Inc.; helium was purified by diffusion through a glass capillary cell supplied by Electron Technology Inc.

X-Ray. The X-ray diffraction patterns were recorded using a Norelco Diffractometer (model number 52019) supplied by the North American Philips Company. A Norelco generator (model number 12045-2) operated at 35 kV and 20 mA provided a source of radiation. In Experiments 1–5, cobalt filtered nickel (K_α) radiation was used but the radiation in Experiment 12 was nickel filtered copper (K_α). The X-rays were detected using a sodium iodide scintillation counter connected to a Norelco Scintillation Proportional Unit (model number 42234). The diffractometer was operated with 2° diverging and receiving slits at a scan rate of 1°/min and a continuous trace of intensity as a function of 2θ was recorded. X-Ray data for electron radial distribution analysis were taken on a diffractometer using molybdenum radiation (K_α), a 1° divergence slit, Soller slits in the primary beam, a 0.2° receiving slit, a graphite monochromator in the diffracted beam, and a Siemens scintillation counter. The molybdenum tube was operated at 46

kV and 13 mA. The detector system included a pulse height analyzer, scaler, timer and printer. The diffractometer was operated in the slow scan and interval count mode (2 min count, 0.125° interval). The sample was mounted in a horizontal position in a helium atmosphere (to avoid contribution of X-ray scattering by air). The sample holder contained Mylar windows. All X-ray samples were ground to a particle size less than 44 μ and packed into the well of a sample holder.

With modern X-ray diffraction techniques, it is possible to separate the various contributions to peak broadening. A basic concept used to achieve this separation is that broadening caused by strain is dependent upon the order of reflection while the broadening produced by small crystallites is independent of the order of reflection. A powder pattern profile, which has been corrected for instrumental broadening, can be expressed as a Fourier series (*8*),

$$P^l(S)\alpha \sum_{-\infty L}^{\infty} A_L \exp[-2\pi i L(S - S_0)], \quad (1)$$

where

$$S = \frac{2 \sin \theta}{\lambda}, \qquad L = nd_{hkl},$$

and

$P^l(S)$ diffraction power per unit length of Debye–Scherrer ring
2θ diffractometer angle, degrees
λ X-ray wavelength, Å
d_{hkl} spacing between reflecting (hkl) planes, Å
n order of reflection
L distance normal to reflecting planes, Å.

In the Warren–Averbach analysis (*8*) the broadening produced by small crystallites and strains can be separated as follows,

$$A_L = A_L^P A_L^\epsilon \quad (2)$$

$$A_L^p = 1 - \frac{L}{D_e} \quad (3)$$

$$A_L^\epsilon = 1 - 2\pi^2 L^2(\langle \epsilon_L^2 \rangle - \langle \epsilon_L \rangle^2) S_0^2 \quad (4)$$

where

$$\epsilon_L = \left[\frac{\Delta L}{L}\right]_L, \qquad S_0 = \frac{2 \sin \theta_0}{\lambda}$$

giving,

ϵ_L strain component normal to reflecting plane
D_e mean effective particle size, Å
θ_0 Bragg diffraction angle, degrees
P (superscript) particle size broadening
ϵ (superscript) strain broadening.

Following the Warren–Averbach method (*8*), the particle size and strains may be separated by the use of the following equation,

$$\ln A_L = \ln A_L^P - 2\pi^2 L^2(\langle \epsilon_L^2 \rangle - \langle \epsilon_L \rangle^2) S_0^2. \quad (5)$$

The effective particle size Fourier coefficient A_P^L can be obtained by plotting ln A_L against S_0^2 for two orders of reflection and extrapolating to $S_0^2 = 0$.

The mean effective particle diameter can be determined by differentiating Eq. (3) and

$$-\left(\frac{dA_L^P}{dL}\right)_{L=0} = \frac{1}{D_e}. \quad (6)$$

Thus, we plot A_P^L as a function of L and the reciprocal of the slope at $L = 0$ will give the average effective particle size D_e. This will correspond to the intercept of the initial slope with the L-axis, because the Fourier coefficients have been normalized ($A_{L=0}^P = 1$).

Another measure of the line-broadening is the width at half the maximum intensity. This quantity is arbitrary and in the present work the line-broadening is characterized by the Von Laue integral breadth (*9*), which is defined as the integrated area of the diffraction peak divided by the maximum intensity.

$$\beta_I(S) = [\int P^l(S) dS]/[P^l(S_0)]. \quad (7)$$

Warren (*8a*) has shown that integral breadth is related to the Fourier coefficients as follows,

$$\beta_I(S) = 1/\sum_{-\infty L}^{\infty} A_L^P. \quad (8)$$

Assuming that particle size broadening is the predominant effect, then

$$\beta_I(S) = 1/D_I, \tag{9}$$

where D_I is the integral breadth particle size which represents a volume average particle size. This integral breadth particle size differs from the effective particle size D_e, which can be considered as a one dimensional average of the crystallites. The relationship between these two measures of particle size is given by Wagner as (*10*),

$$D_I = \overline{(D_e)^2}/\bar{D}_e \tag{10}$$

Since $D_I/\bar{D}_e = \overline{(D_e)^2}/(\bar{D}_e)^2 \geq 1$ or $D_I \geq \bar{D}_e$, we expect the integral breadth crystallite size to be larger, never smaller, than the average effective particle size.

The diffraction results were analyzed using a computer program supplied by Wagner (*11*). First the measured profiles were corrected for polarization and geometric factors, and the 2θ scale was converted to equal intervals in S-space. The peak profile was used to determine the position of the peak maximum and the lattice parameter corresponding to the (*hkl*) reflection. The Fourier coefficients were calculated for both the sample and standard (macrocrystalline α-Cr_2O_3) diffraction profiles at different values of L normal to the reflecting planes. Allowance was made for instrumental broadening using the method of Stokes (*12*). The Fourier coefficients were then used to separate particle size and strain using Eq. (5). The average effective particle size D_e was obtained from a computer plot of A_L vs. L. The integral breadth obtained from Eq. (8) was corrected for instrumental broadening using the following empirical parabolic relationship (*10*).

$$\beta_{\text{CORR}} = \beta_{\text{MEAS}} - (\beta_{\text{STD}})^2/\beta_{\text{MEAS}} \tag{11}$$

β_{CORR} corrected integral breadth
β_{MEAS} integral breadth from measured diffraction profile
β_{STD} integral breadth from diffraction profile for standard sample (macrocrystalline α-Cr_2O_3).

The effective integral breadth D_I was calculated from Eq. (9).

The derivation of the electron radial distribution from X-ray scattering theory has been reviewed by Wagner (*13*) for a binary system containing different elements. The intensity of coherent X-ray scattering per atom (coh) [in electron units (eu)] due to more than one kind of atom is,

$$I_{\text{eu}}^{\text{coh}}(K) = \langle f^2\rangle + \langle f\rangle^2 \int_0^\infty 4\pi r[\rho(r) - \rho_0] \times \frac{\sin Kr}{K}\, dr \tag{12}$$

where

$$K = 4\pi \sin\theta/\lambda$$
$$\langle f\rangle = (C_a f_a + C_b f_b)$$
$$\langle f^2\rangle = (C_a f_a^2 + C_b f_b^2) = \langle f\rangle^2 + C_a C_b (f_a - f_b)^2$$
$$\rho(r) = \frac{C_a f_a^2 \rho_{aa}(r) + C_b f_b^2 \rho_{bb}(r) + 2C_a f_a f_b \rho_{ab}(r)}{(C_a f_a + C_b f_b)^2}$$

and

C_a atomic fraction of atom a
C_b atomic fraction of atom b
f_a scattering factor of atom a (*14*)
f_b scattering factor of atom b (*14*)
r radial distance, Å
ρ_0 average density = 5.21 g/cm³ (*15*)
$\rho(r)$ weighted electron radial density function for each component present.

Therefore the coherent scattering per atom becomes,

$$I_{\text{eu}}^{\text{coh}}(K) = C_a C_b (f_a - f_b)^2 + (C_a f_a + C_b f_b)^2 \times \left\{1 + \int_0^\infty 4\pi r[\rho(r) - \rho_0] \frac{\sin Kr}{K}\, dr\right\}.$$

The interference function $I(K)$ is defined as,

$$I(K) = 1 + \int_0^\infty 4\pi r[\rho(r) - \rho_0] \frac{\sin Kr}{K}\, dr. \tag{13}$$

Substituting into Eq. (12) gives

$$I(K) = \frac{I_{\text{eu}}^{\text{coh}}(K) - C_a C_b (f_a - f_b)^2}{(C_a f_a + C_b f_b)^2} \tag{14}$$

The reduced intensity function,

$$F(K) = K[I(K) - 1] = \int_0^\infty 4\pi r[\rho(r) - \rho_0] \sin Kr\, dr, \quad (15)$$

can be inverted by a Fourier transformation to give the reduced radial distribution function,

$$G(r) = 4\pi r^2[\rho(r) - \rho_0] = \frac{2r}{\pi} \int_0^\infty F(K) \sin Kr\, dK. \quad (16)$$

The experimental intensities are given by

$$I_{MEAS}(K) \alpha I_{eu}^{coh}(K) + C_a C_b (f_a - f_b)^2 + I_{eu}^{incoh}(K), \quad (17)$$

where $I_{eu}^{incoh}(K)$ is the Compton scattering and $C_a C_b (f_a - f_b)^2$ is the Laue monotonic scattering term.

The X-ray intensity data from catalyst A were analyzed by a computer program supplied by Wagner (*16*). The measured intensities were corrected for background, polarization, and absorption which are characteristic of the diffraction geometry. The interference function $I(K)$ is calculated from Eq. (14) and the F(K) curves from Eq. (15). The radial distribution function was evaluated after calculation of the Fourier coefficients according to Eq. (16). The input for the calculation of $<f>^2$ consists of scattering factors for chromium (III) and oxide ion taken from published tables (*14*). Corrections for the Compton scattering were based on literature values for each element (*17*).

Electron microscopy. Electron-transmission micrographs were taken on an Associated Electrical Industries EM6G electron microscope at an accelerating voltage of 30 kV. The specimens were prepared using a technique described by Hall (*18*). The catalyst was crushed to a fine powder and after small particles were dusted onto a glass slide coated with Formvar film, the film was floated onto the surface of distilled water. Copper electron microscope grids were placed over the catalyst powder and a glass slide was used to pick up the grid, the sample being between the grid and the Formvar coating. The chromium oxide specimens were viewed at a magnification of 10,000 and the micrographs were photographically enlarged (Fig. 6—5.5×; Fig. 7—7×). Electron diffraction patterns were also measured for all specimens which were examined by transmission.

Infrared spectroscopy. Infrared spectra of the catalyst were obtained using the pellet technique. Physical mixtures containing approximately 0.4 wt % chromium oxide, 1% potassium nitrate standard and 98.6% potassium bromide were prepared. The grain sizes were reduced to 44 μ in an agate mortar in order to minimize reflections and refractions at the faces of the solid particles. The mixture was placed in an aluminum foil frame and compressed in a die under a pressure of approximately 1000 atm. After the pellet was removed from the die, a transmission spectrum was recorded on a Beckman IR 12 Infrared spectrometer with a blank potassium bromide pellet in the reference beam. The potassium nitrate standard was used to correct for variation in the pellet thickness. The per cent crystallinity was determined from the absorbance at 620 cm^{-1} (*4*) by comparison with a calibration curve obtained using mixtures of pure amorphous and pure macrocrystalline chromium oxide.

Nitrogen isotherms. Nitrogen adsorption and desorption isotherms at liquid nitrogen temperature were obtained using an Englehard Industries, Inc. Isorpta Analyzer model 2A, a dynamic sorptometer equipped with a thermal conductivity detector. A sample of 0.5–0.75 g was sealed into the flow system outgassed at 200°C in flowing helium before proceeding with adsorption measurement. The surface area was calculated from the nitrogen adsorption data using the linear form of the Brunauer–Emmett–Teller equation (*19*). A micropore size distribution was calculated from the nitrogen isotherms by the method of Barrett, Joyner, and Halenda (*20*). This method also permitted the calculation of the cumulative surface area and the specific pore volume for the catalyst. A computer program devised by Irving (*21*) was used for this computation. The average micropore radius is obtained from a plot of $\Delta v/\Delta r$ against r where Δv is a change in

pore volume corresponding to a change in pore radius, Δr.

Results and Discussion

In an attempt to prepare catalyst C with varying microcrystallite size, we followed the procedure outlined in the experimental section but varied the 12 hr holding temperature above and below 400°C. When the holding temperature was lowered by as little as 8°C below 400°C no crystallization was observed. The average effective crystallite size D_e and effective integral breadth D_I for six catalysts obtained with a holding temperature of 400°C or above are given in Table 1. These experiments suggest that nucleation occurs over a very narrow temperature range. Once initiated, crystal growth of α-Cr_2O_3 (no other phase or composition was observed) continues until an average effective crystallite size of about 80 Å is reached. When the pressure of hydrogen is decreased, the temperature at which crystallization is initiated is increased but the distribution of crystallite sizes is probably not affected. (For example, in 100 Torr of hydrogen the crystallization occurs above 425°C) (*22*). Thus, it appears unlikely that chromia catalysts with crystallites in the critical range 15–70 Å (*5*) can be prepared using unsupported chromia.

TABLE 1
Crystallite Sizes of Chromia Catalyst C

Experiment	Holding temperature (°C)	*hkl* of diffraction peak	D_e (Å)	D_I (Å)
1	400	104	72	90
		110	88	153
		116	83	109
2	410	104	77	100
		110	130	184
		116	98	118
		012	100	139
		024	107	114
3	420	104	89	101
		110	127	197
		116	100	120
		012	124	172
		024	130	165
4	430	104	88	109
		110	158	228
		116	98	118
5	440	104	86	113
		110	136	213
		116	97	128
		012	122	155
		024	115	143
12	450	104	110	143
		110	194	263
		116	113	152

The results presented in Table 1 permit us to make some qualitative statements about the shape of the microcrystallites by comparing the average crystallite sizes measured using different diffraction peaks. The average size as determined from the broadening of the (110) diffraction peak is a measure of the dimension in the a-direction (along one of the three a-axes in the hexagonal coordinate system) while the size measured by the (116) diffraction peak is a rough approximation of the length along the c-axis (normal to the plane of the a-axes). Keeping in mind that D_e is a one-dimensional average while D_I is a volume average (and thus is weighted in favor of large crystallites) we can make the following observation about the shape–size relationship. Crystallites which have a dimension less than 100 Å in the a-direction appear to be more or less spherical (see D_e of Experiment 1, Table 1) while those which are greater than 100 Å in the a-direction tend to grow toward platelets which have a diameter about twice their thickness (see D_I of Experiment 1, or D_e and D_I of Experiments 2–12, Table 1). A similar shape is observed when the crystals are grown to micron size (*23*). We can make one additional observation concerning the nature of microcrystallites of α-Cr_2O_3 from the data presented in Table 1. Since we have seen that there may be a contribution to the line-broadening due to bulk strain in addition to that expected from the small crystallites, the fact that the average crystallite size as measured by the (012) and (024) reflections is the same within experimental error (± 10 Å) indicates that the microcrystallites are essentially strain free along the direction normal to these planes.

In Fig. 1 the integral breadth crystallite size measured by the (110) reflection (a measure of length in the preferential growth direction) and the per cent crystallinity measured by infrared absorption are plotted against the holding temperature. Both show a near linear relationship (excluding the crystallinity point at 420°C). This correlation between the volume average size and volume per cent crystallinity is to be expected if most of the crystal growth centers are nucleated at 400°C and increased temperature causes the crystals to grow in size but does not produce new growth centers. It should be noted that even for the most crystalline catalysts which still retain a reasonable surface area more than half the chromium oxide remains amorphous. Thus, catalyst C can be considered to be microcrystalline chromia supported on amorphous chromia.

Let us now consider the structure of catalyst A, "amorphous chromium oxide." The radial distribution function for this material (used in Experiment 16) is shown in Fig. 2(a) and is presented in tabular form in Table 2. The first peak in the distribution curve at 2 Å is not unexpected. It is due to the oxygen nearest neighbors and would be observed even in the hydrated ion, $[Cr(H_2O)_6]^{3+}$. However, the close correlation between the four nearest neighbor Cr–Cr distances of bulk α-Cr_2O_3 and those observed in catalyst A is somewhat surprising. It should be noted that the Cr–Cr distances of catalyst A do not correlate with those of CrOOH (*24*). This is an important observation since amorphous chromia catalysts prepared at 400°C retain considerable water and thermogravimetric analysis in air indicate that the monohydrate is stable between 280 and 360°C (*25*). It must be concluded that the retained water constitutes surface hydroxyls as previously postulated.

The various kinds of interatomic distances found in α-Cr_2O_3 are given in the first column of Table 2 and are illustrated in Fig. 3, a projection along the a_1-axis onto the $(2\bar{1}0)$ plane taken from Newnham (*26*). The number of nearest neighbors of a given kind is proportional to the area under peaks in the distribution curve. From $\rho(r)$ defined in Eq. (12), we write

$$4\pi r^2\rho(r) = 4\pi r^2\left[\frac{C_{Cr}f_{Cr}^2\rho_{Cr-Cr}(r) + C_Of_O^2\rho_{O-O}(r) + 2C_{Cr}f_{Cr}f_O\rho_{Cr-O}(r)}{(C_{Cr}f_{Cr} + C_Of_O)^2}\right]. \quad (18)$$

If we consider only the first peak in Fig. 2(a) we can set $\rho_{Cr-Cr}(r) = \rho_{O-O}(r) = 0$, re-

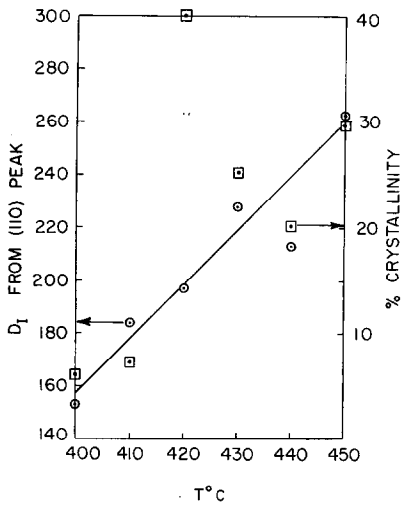

FIG. 1. Integral breadth particle size measured from the (110) diffraction peak and per cent crystallinity versus the catalyst activation temperature.

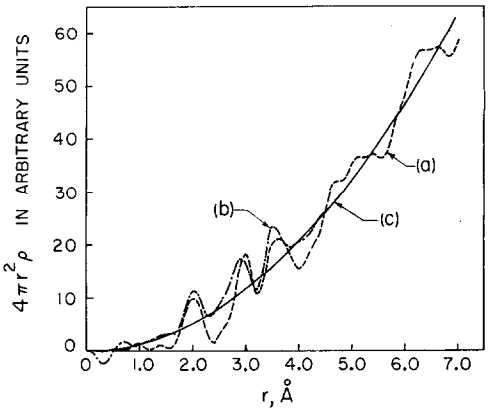

FIG. 2. (a) Radial distribution curve for catalyst A, Experiment 16, (b) radial distribution curve for Cr_3O_{12} model, and (c) a uniform distribution.

TABLE 2
COMPARISON OF INTERATOMIC DISTANCES OF α-Cr_2O_3 AND CATALYST A

α-Cr_2O_3[a] (Å)	Number of nearest neighbors[a]	Assignment of bonds,[a] (see Fig. 3)	Catalyst A (Å)	Approx. number of nearest neighbors[b]
1.97	3	Cr_1–O_1	2	6
2.02	3	Cr_1–O_5		
2.65	1	Cr_1–Cr_2	2.6	1
2.89	3	Cr_1–Cr_3	3.0	6
3.43	3	Cr_1–Cr_4	3.6	6
3.65	6	Cr_1–Cr_5		
2.63	2	O_1–O_2		
2.99	4	O_1–O_3		
2.74	2	O_1–O_4		
2.85	4	O_1–O_5		

[a] From ref. *26*. [b] See text for explanation.

arrange and integrate in order to determine the approximate average oxygen coordination number (CN) for chromium,

$$CN_{Cr-O} = 4\pi \int_{r=0}^{r=2.4} r^2 \rho_{Cr-O}(r)\, dr = \frac{4\pi(C_{Cr}f_{Cr} + C_O f_O)^2}{2C_{Cr}f_{Cr}f_O} \int_{r=0}^{r=2.4} r^2 \rho(r)\, dr = 6.3 \approx 6. \quad (19)$$

It should be noted that the CN_{Cr-O} for the active form of catalyst A is probably less than six, since the sample used to obtain the X-ray scattering curve was exposed to the atmosphere and, presumably, had adsorbed sufficient water to attain octahedral coordination about each chromium. If we proceed in a similar manner with each of the chromium–chromium peaks of Fig. 2(a) and allow for the oxygen–oxygen scattering which contributes intensity in the 2.6–3 Å region of the distribution curve (the method used to estimate the oxygen–oxygen intensity is discussed below), we calculate an average number of nearest neighbor

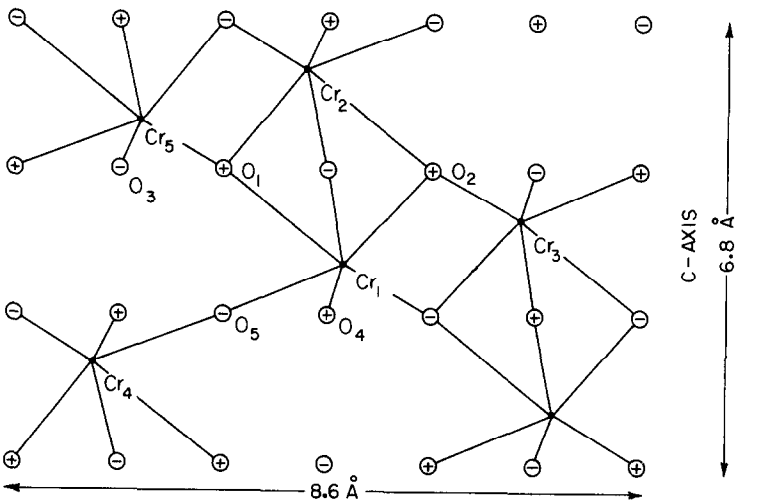

FIG. 3. A projection of the α-Cr_2O_3 structure along the a_1-axis onto the $(2\ \bar{1}\ 0)$ plane. The chromium (III) ions, ●, are in the plane and oxygen ions, ○ are above and below the plane. After R. E. Newnham and Y. M. de Haan (*26*).

chromiums to be in ratio of roughly 1:6:12 for Cr_1–Cr_2, Cr_1–Cr_3, and Cr_1–Cr_4 + Cr_1–Cr_5, respectively (see Fig. 3). We can now construct a model which is consistent with this experimental result in the following manner. As a basis for our model, we begin with Cr_1, Cr_2, Cr_3, and Cr_5 of Fig. 3 and add a third dimension to complete the trigonal symmetry (relative to the *c*-axis) about Cr_1 and Cr_2 by adding four more chromium (III) ions, two above and two below the plane of projection. The twelve oxygen ions needed for electrical neutrality are arranged to maximize the chromium coordination number, they are stacked three above Cr_1, three below Cr_2, and six between Cr_1 and Cr_2. A projection of this structure on to the (001) plane is given in Fig. 4. If this structure were extended along the hexagonal *c*-axis, it would be essentially identical to the filamentous model proposed by Selwood *et al.* (*27*) to account for the magnetic properties of hydrous chromium oxide. The three chromium around Cr_1 will all be spaced at the Cr_1–Cr_3 distance and the three around Cr_2 will be spaced at the Cr_2–Cr_5 distance which is equal to the Cr_1–Cr_3 distance. Thus, the unit Cr_8O_{12} has the correct ratio of Cr_1–Cr_2 to Cr_1–Cr_3 distances of 1:6. Closer scrutiny shows that it also has 6 Cr_1–Cr_4 spacings and 6 Cr_1–Cr_5 spacings to make up the required 12. Now, using the Debye (*28*) scattering equation,

$$I(K) = \sum_m \sum_n f_m f_n \frac{\sin Kr_{mn}}{Kr_{mn}} \qquad (20)$$

where r_{mn} is the distance between atoms m and n and all other terms are defined in Eq. (12), we can write down an expression for the intensity expected from our small crystallite, Cr_8O_{12},

An average value of 2.00 Å for r(Cr–O) and appropriate values from Table 2 were used in Eq. (21) to calculate an intensity vs. scattering angle curve. From this intensity data, a radial distribution curve, Fig. 2(b), was calculated using the same program used to analyze the experimental data (without correction for Compton scattering). The actual calculation gives $4\pi r^2 (\rho'(r) + \rho_0)$ [where $\rho'(r)$ results from the Cr_8O_{12} "crystal" and ρ_0 is the density of α-Cr_2O_3] and not $4\pi r^2 \rho(r)$ as in the case of the experimental data so that the two curves cannot be quantitatively compared. But the result of Fig. 2(b) does suggest that the model is a fair representation of the local order in catalyst A except that all chromium–chromium distances of catalyst A are larger by 3–4%. The model can also be used to estimate the contribution to the radial distribution curve from oxygen–oxygen scattering. This is done by repeating the calculation without the oxygen–oxygen scattering and comparing the resulting curve to Fig. 2(b) as is done in Fig. 5. Not all of the chromium–chromium distances necessary to describe the model were included in Eq. (21). For example, the distance Cr_3–Cr_5 (see Fig. 3) and the distance between Cr_3 and its equivalent at $\pm 120°$ around the *c*-axis (see Fig. 4) would account for the peaks around 5 Å on the experimental radial distribution curve. From this analysis we conclude that catalyst A has local order of the same kind as α-Cr_2O_3 over approximately a 10 Å dimension.

Electron micrographs of both forms of chromia catalysts are shown in Figs. 6 and 7. These are strikingly similar to Figs. 6a and 6b shown by Cross and Leach (*29*). They prepared their amorphous sample by

$$I(K) = 8f_{Cr}^2 + 12f_O^2 + 60f_{Cr}f_O \frac{\sin Kr\,(Cr\text{–}O)}{Kr\,(Cr\text{–}O)} + \frac{2f_{Cr}^2 \sin Kr\,(Cr_1\text{–}Cr_2)}{Kr\,(Cr_1\text{–}Cr_2)} + \frac{12f_{Cr}^2 \sin Kr\,(Cr_1\text{–}Cr_3)}{Kr\,(Cr_1\text{–}Cr_3)} + \frac{12f_{Cr}^2 \sin Kr\,(Cr_1\text{–}Cr_4)}{Kr\,(Cr_1\text{–}Cr_4)} + \frac{12f_{Cr}^2 \sin Kr\,(Cr_1\text{–}Cr_5)}{Kr\,(Cr_1\text{–}Cr_5)} + \frac{18f_O^2 \sin Kr\,(O_1\text{–}O_2)}{Kr\,(O_1\text{–}O_2)} + \frac{36f_O^2 \sin Kr\,(O_1\text{–}O_3)}{Kr\,(O_1\text{–}O_3)} + \frac{18f_O^2 \sin Kr\,(O_1\text{–}O_4)}{Kr\,(O_1\text{–}O_4)} + \frac{36f_O^2 \sin Kr\,(O_1\text{–}O_5)}{Kr\,(O_1\text{–}O_5)}. \qquad (21)$$

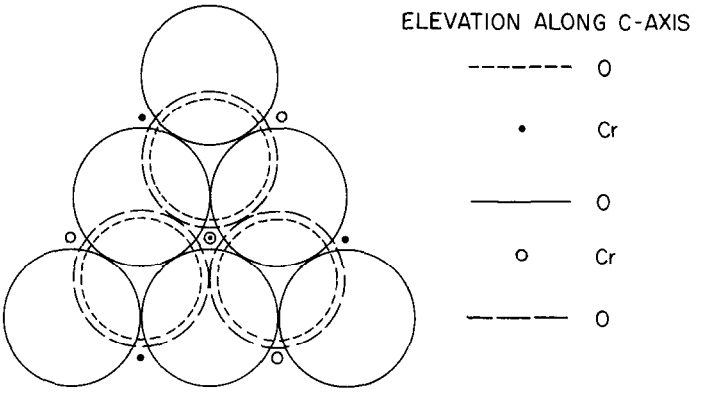

FIG. 4. A projection of the Cr_8O_{12} model along the c-axis onto the (001) plane. The positions of the three oxygen planes and two chromium planes are given in elevation.

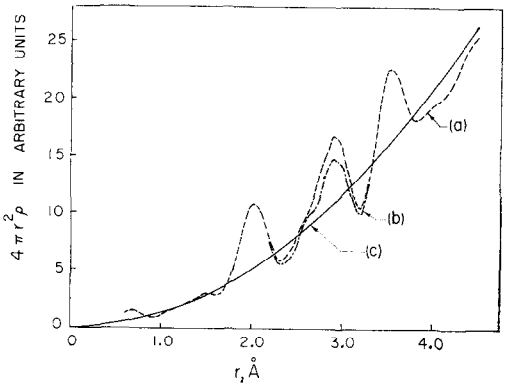

FIG. 5. (a) Radial distribution curve for Cr_8O_{12} model (same as Fig. 2b), (b) radial distribution curve for Cr_8O_{12} neglecting oxygen–oxygen scattering, and (c) a uniform distribution.

outgassing in air at 364°C and their microcrystalline sample by outgassing in air at 431°C. Although the catalyst form can be immediately recognized by its micrograph, little new information is obtained with the resolution attained in this work. The crystalline catalyst appears to have a very open structure with grain sizes approaching 150 Å which is consistent with the crystallite sizes shown in Table 1. Likewise, no additional information was obtained from the electron diffraction patterns. Samples which diffract X-rays always give electron diffraction patterns and those which do not give an X-ray diffraction pattern show the same behavior with electrons. This is in contrast with the work of Burzyk *et al.*

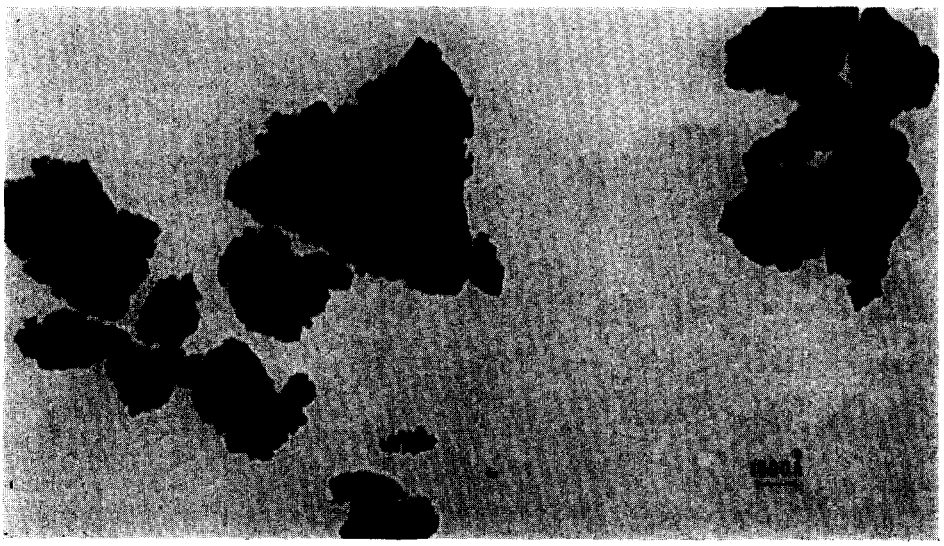

FIG. 6. Electron micrograph of catalyst A.

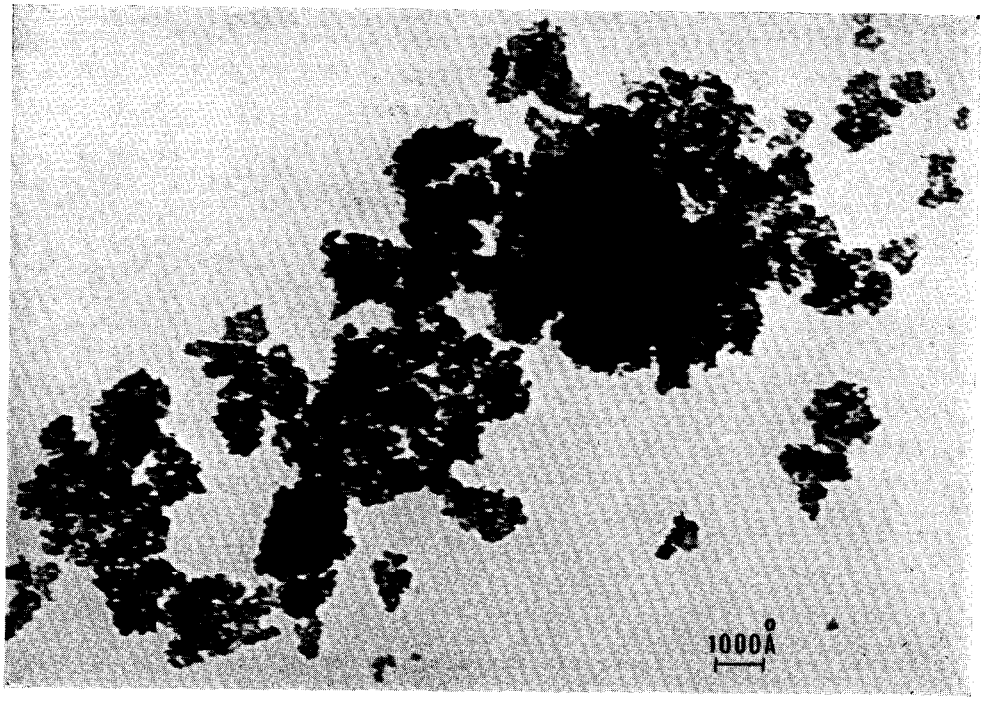

FIG. 7. Electron micrograph of catalyst C.

(*30*) where electron diffraction patterns were reported for samples which did not display X-ray diffraction patterns.

We conclude our discussion of the structure of chromia catalysts with a few comments on the macroscopic structure of these catalysts determined from the low temperature nitrogen isotherms. Figure 8 shows the change in BET surface area with increased holding temperature; these curves

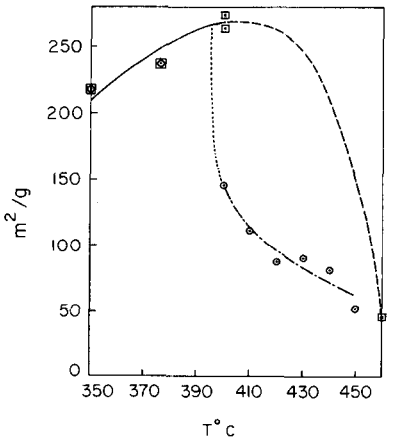

FIG. 8. BET surface area as a function of activation temperature, ⊡ in helium; ⊙ in hydrogen.

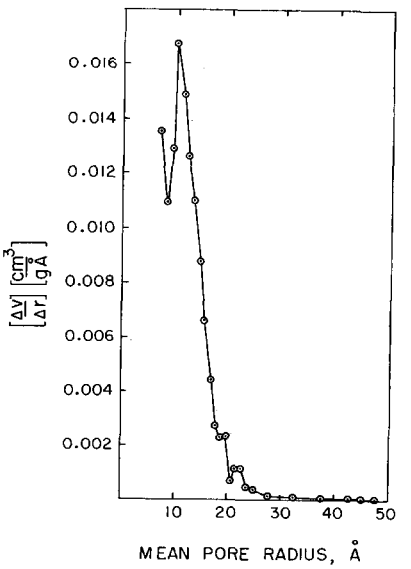

FIG. 9. Pore size distribution for catalyst A calculated from the data of Taylor (*22*).

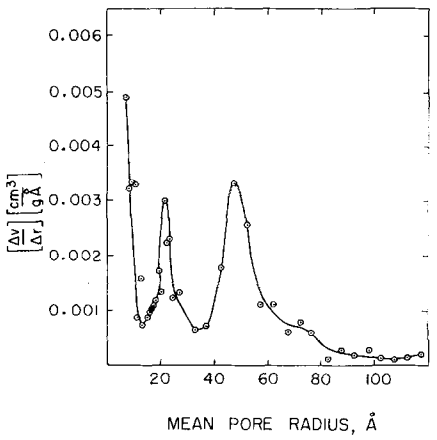

FIG. 10. Pore size distribution for catalyst C calculated from the data of Taylor (*22*).

are very similar to curves reported previously (*4*, *29*). Taylor (*22*) reported pore diameters calculated from *t*-plots of de Boer and Lippens (*31*) for catalyst A and C as 12 and 52 Å, respectively. We have obtained similar results using the Barrett, Joyner and Halenda method (*20*). Our catalysts do not differ significantly from those prepared by Taylor and, therefore, in Figs. 9 and 10 we present radial pore-size distributions calculated from Taylor's data. Whatever method is used, there is a general agreement that catalyst A has very narrow micropores which increase in diameter when the catalyst is converted to form C while the porosity remains nearly constant at about 0.12 cm^3/g (*4*, *29*, *32*). It is important to be aware of these changes in macroscopic structure when we attempt to interpret the effect on catalytic activity that accompanies the catalyst atomic structural change from crystallographic order over 10 Å dimension (form A) to crystallographic order over a 100 Å dimension (form C).

ACKNOWLEDGMENTS

Fellowship support for S. R. Dyne was provided by Standard Oil Company of California, The South African Council for Scientific and Industrial Research and NSF Grant No. GK1014. Computer programs for the X-ray analysis and helpful discussion of the results by C. N. J. Wagner are gratefully acknowledged. We also wish to thank G. S. Cargill for his useful discussion of the radial distribution curves.

REFERENCES

1. BOUDART, M., *in* "Advances in Catalysis," (W. G. Frankenburg, V. I. Komarewsky, and E. K. Rideal, eds.), Vol. 20, p. 153. Academic Press, New York, 1969; references cited therein.
2. (a) COSSEE, P., *J. Catal.* **3**, 80 (1964); (b) ARLMAN, E. J., *J. Catal.* **3**, 89 (1964); (c) ARLMAN, E. J., AND COSSEE, P., *J. Catal.* **3**, 99 (1964); (d) COSSEE, P., ROS, P., AND SCHACHTSCHNEIDER, J. H., *Int. Congr. Catal. 4th.*, Moscow, paper 14 (1968).
3. (a) VENUTO, P. B., AND LANDIS, P. S., *in* "Advances in Catalysis" (W. G. Frankenburg, V. I. Komarewsky, and E. K. Rideal, eds.), Vol. 18, p. 259. Academic Press, New York, 1968; (b) PANCHENKOV, G. M., AND KOLESNIKOV, I. M., *Russ. J. Phys. Chem.* **44**, 500 (1970), see also references cited in these reviews.
4. BURWELL, R. L., JR., HALLER, G. L., TAYLOR, K. C., AND READ, J. F., "Advances in Catalysis" (W. G. Frankenburg, V. I. Komarewsky, and E. K. Rideal, eds.), Vol. 20, p. 1. Academic Press, New York, 1969.
5. (a) POLTORAK, O. M., AND BORONIN, V. S., *Int. Chem. Eng.* **7**, 452 (1967); (b) VAN HARDEVELD, R., AND HARTOG, F., *Surface Sci.* **15**, 189 (1969).
6. DYNE, S. R., BUTT, J. B., AND HALLER, G. L., *J. Catal.* **25**, 391 (1972).
7. PASS, G., LITTLEWOOD, A. B., AND BURWELL, R. L., JR., *J. Amer. Chem. Soc.* **82**, 6281 (1960).
8. (a) WARREN, B. E., *Progr. Met. Phys.* **8**, 147 (1958); (b) WARREN, B. E., "X-Ray Diffraction." Addison-Wesley, Reading, MA, 1969.
9. VON LAUE, M., *Z. Kristallogr. Mineral.* **64**, 115 (1926).
10. WAGNER, C. N. J., *Met. Soc. Conf.* **36**, 219 (1965).
11. WAGNER, C. N. J., "A FORTRAN IV Program for the Analysis of Positions and Profiles of X-ray Powder Pattern Peaks," Office of Naval Research Contract NONR-609 (43) Technical Report No. 15 (1966).
12. STOKES, A. R., *Proc. Phys. Soc.* (London), **B61**, 382 (1948).
13. (a) LIGHT, T. B., AND WAGNER, C. N. J., *J. Appl. Crystallogr.* **1**, 199 (1968); (b) WAGNER, C. N. J., *Vac. Sci. Technol.* **6**, 650 (1969); (c) WAGNER, C. N. J., LIGHT, T. B.,

HALDER, N. C., AND LUKENS, W. E., *J. Appl. Phys.* **39**, 3690 (1968).

14. (a) CROMER, D. T., AND WABER, J. T., *Acta Crystallogr.* **18**, 104 (1965); (b) CULLITY, B. D., "Elements of X-ray Diffraction," Appendix 8, Addison-Wesley, Reading, MA, 1956.

15. We have removed the small angle scattering by an exponential extrapolation to zero from $2\theta = 6°$. In this case the correct density is that of the single crystal rather than the bulk density of the powder sample. See CARGILL, G. S., III, *J. Appl. Crystallogr.* **4**, 277 (1971).

16. WAGNER, C. N. J., "A FORTRAN IV Program for the Calculation of the Radial Distribution Function of Binary Alloys," National Science Foundation Grant G. P. 3213, Technical Report No. 2 (1966).

17. SAGEL, K., "Tabellen zur Röntgenstrukturanalyze." Springer-Verlag, Berlin, 1958.

18. HALL, C. E., "Introduction to Electron Microscopy," 2nd ed. McGraw-Hill, New York, 1966.

19. GREGG, S. J., AND SING, K. S. W., "Adsorption, Surface Area and Porosity." Academic Press, London, 1967.

20. BARRETT, E. P., JOYNER, L. G., AND HALENDA, P. P., *J. Amer. Chem. Soc.* **73**, 373 (1951).

21. IRVING, J. P., Ph.D. thesis, Yale Univ. New Haven, CT, 1966.

22. TAYLOR, K. C., Ph.D. thesis, Northwestern Univ., Evanston, IL, 1968.

23. YAO, Y.-F. Y., *J. Phys. Chem.* **69**, 3930 (1965).

24. DOUGLASS, R. M., *Acta Crystallogr.* **10**, 423 (1957).

25. DEREN, J., HABER, J., PODGORECKA, A., AND BURZYK, J., *J. Catal.* **2**, 161 (1963).

26. NEWNHAM, R. E., AND DE HAAN, Y. M., *Z. Kristallogr. Mineral.* **117**, 235 (1962).

27. SELWOOD, P. W., ELLIS, M., AND DAVIS, C. F., JR., *J. Amer. Chem. Soc.* **72**, 3549 (1950).

28. DEBYE, P., *Ann. Phys.* **46**, 809 (1915).

29. CROSS, N. E., AND LEACH, H. F., *J. Catal.* **21**, 239 (1971).

30. BURZYK, J., DEREN, J., AND HABER, J., *Reactiv. Solids Int. Symp. 5th* (1964).

31. DE BOER, J. H., LIPPENS, B. C., LINSEN, B. G., BROCKJOFF, J. C. P., VAN DEN HEUVEL, H., AND OSINGA, T. H., *J. Colloid Sci.* **21**, 405 (1966), and references therein.

32. BURWELL, R. L., JR., TAYLOR, K. C., AND HALLER, G. L., *J. Phys. Chem.* **71**, 4580 (1967).